Journal of Optoelectronic and Biomedical Materials Vol. 17, No. 4, October-December 2025, p. 251-261

Nickel-vanadium bimetallic phosphide derived from layered double hydroxide: a high-performance electrocatalyst for selective hydroxylation of phenol to hydroquinone

Y. Xu *, X. Yang, L. Gan, J. Liu
College of Materials Science and Engineering, Key Laboratory of New Processing Technology for Nonferrous Metals and Materials, Ministry of Education, Guilin University of Technology, Guilin 541004, China

Replacing energy-intensive thermal synthesis, we report a green electrocatalytic strategy for phenol hydroxylation to hydroquinone (HQ) using a novel Ni-V bimetallic phosphide (P-NiV) catalyst. Synthesized via phosphating NiV-LDH, P-NiV exhibits enhanced conductivity, stability, and active site regulation, confirmed by SEM/XRD. Under optimal conditions (0.5 V vs RHE, 40°C), P-NiV achieved 57.7% phenol conversion and 62% HQ selectivity. This electrocatalytic approach significantly lowers energy consumption and operating temperature compared to thermal methods, offering a sustainable alternative for industrial HQ production.

(Received August 13, 2025; Accepted October 27, 2025)

Keywords: Hydroxylation of phenol, Layered double hydroxide, Electrocatalysis, Transition metal phosphide, Topological transformation

1. Introduction

Hydroquinone (HQ), together with its isomers catechol and resorcinol, is utilized as a pivotal reaction intermediate in the generation of fragrances, dyes, pharmaceuticals, and rubber additives.[1] However, conventional industrial synthetic methods—primarily aniline oxidation and cumene oxidation—are associated with complex production processes, reliance on toxic auxiliary reagents, and generation of a large amount of hazardous waste, all of which pose significant environmental and safety concerns. As an alternative, Atom-economic hydroxylation of phenol directly yielding HQ in one catalytic step is widely acknowledged as a promising and environmentally friendly approach.[2-4] Nevertheless, the inherent conjugation of the aromatic ring renders phenol highly stable, and selective hydroxylation remains challenging due to poor catalyst reusability and rapid deactivation.

Electrocatalytic oxidation for phenol hydroxylation, as an alternative to traditional thermal and photocatalytic strategies enabling the in-situ generation of highly reactive radical species via single-electron transfer pathways, has attracted increasing attention. In this method, electrons act as clean oxidants, selectively activating the inert Csp^2–H bonds under mild conditions and guiding the transformation toward HQ.[5] However, current systems frequently rely on noble metal catalysts to achieve sufficient C–H activation efficiency, which leads to high material costs and limits scalability. Therefore, developing efficient, non-noble metal electrocatalysts is of great significance.[6, 7]

Vanadium (V), an earth-abundant transition metal, exhibits multiple valence states and unsaturated 3d orbitals, making it suitable for Csp^2–H bond activation through strong coordination interactions.[8-12] V-based electrode materials, such as V_2O_5-derived metal oxides, have been investigated for the electrochemical oxidation of benzene to phenol, achieving high selectivity (up to 94.7%), but suffering from low overall yields due to limited active surface area.[8] In addition, the monometallic V-based catalyst system face two major drawbacks: high intrinsic activation barriers and poor charge transfer efficiency, both of which significantly hinder catalytic performance.

* Corresponding author: xuyanqi@glut.edu.cn
https://doi.org/10.15251/JOBM.2025.174.251

To address these limitations, bimetallic synergistic strategies have been proposed. In particular, nickel (Ni), with its partially filled 3d orbitals, readily undergoes charge redistribution with vanadium ions, thereby enhancing electron transfer and overall activity.[13-15] Furthermore, the slim energy separation within the d-band center of Ni atoms and the Fermi energy level promotes the adsorption of intermediates in thermodynamic reactions,[16] while the occurrence of Ni substantially improved the long-term performance retention of the electrode materials.[17] Layered double hydroxides (LDHs), as a distinctive class of 2D layered anionic materials, have the general formula of composition as follows: $[M^{2+}_{1-x}\ M^{3+}_{x}(OH)_2]^{x+}(A^{n-})_{x/n}\cdot mH_2O$, where M^{2+} denotes divalent metallic ions, M^{3+} represents trivalent metal ions, and A^{n-} signifies charge-balancing interlayer anions. On account of their adjustable metal composition, enhanced interfacial area with high density of active centers, LDHs has been regarded as a versatile platform for electrocatalyst design. However, LDHs often suffer from poor electrochemical stability due to structural collapse or surface oxidation during electrocatalysis. Modification of LDHs by topological transformation, such as calcination or phosphating, can effectively modulate their electronic structure and surface defects, thereby enhancing catalytic activity and durability.[18] Despite the demonstrated promise of bimetallic phosphides derived from LDHs in electrocatalytic phenol hydroxylation remains underexplored.

Herein, the HQ was efficiently synthesized via electrocatalytic oxidation hydroxylation of phenol using a P-NiV catalyst derived from the NiV-LDH precursor by phosphating treatment. This structural modification, yielding P-NiV catalyst with increased surface-active sites, significantly promoted the adsorption and activation of para-substituted phenol molecules, resulting in boosting the performance of the electrocatalytic hydroxylation process. The formation of HQ as the target product was verified by high-performance liquid chromatography (HPLC). Among the synthesized catalysts, P-NiV exhibited superior phenol conversion and HQ selectivity. Specifically, the optimal conditions for phenol conversion were identified under potentiation control at 0.7 V and a reaction temperature of 50 °C, while the highest HQ selectivity was achieved at 0.5 V under room temperature.

2. Experimental

2.1. Materials

Formamide were bought from Aladdin Biochemistry Technology (Shanghai, China) Co., Ltd. VCl_3 were gotten from Shanghai Finding Biotechnology Co., Ltd. $(Ni(NO_3)_2{\cdot}6H_2O$ and HCl were procured from Shantou Xilong Chemical Reagent Co., Ltd. $NaNO_3$, KOH, NaOH, and ethanol were acquired from Sichuan Xilong Science Co., Ltd. NaH_2PO_2 were sourced from RON's Reagent Company. Phenol and hydroquinone (HQ) were sourced from Shanghai Yien Chemical Technology Co., Ltd. KBr were sourced from Sinopharm Group Chemical Reagent Co., Ltd. Nafion solution (5%) was sourced from Shanghai DuPont Chemical Group Co., Ltd. The aforementioned reagents were used without further purification.

2.2. Characterizations

X-ray diffraction (XRD) patterns were acquired using an X' Pert PRO diffractometer with Cu Kα radiation (λ = 1.5405 Å). Fourier transform infrared (FTIR) (500–4000 cm^{-1}) spectra were recorded on a Nicolet 205 Infrared Spectrometer. Field-emission scanning electron microscopy (FE-SEM) images were obtained with a Hitachi S-4800 instrument. Energy dispersive X-ray spectroscopy (EDS) was applied for qualitative and statistical assessment of each element in the catalyst (the X-ray energy spectrometer attached to the S-4800 scanning electron microscope).

2.3. Synthesis of NiV-LDH, NiV-LDO, and P-NiV

Nickel–vanadium layered double hydroxide (NiV-LDH) was prepared by a coprecipitation method.[19] Under magnetic stirring at 80 °C, 10.0 mL of a mixed metal ion solution containing $Ni(NO_3)_2{\cdot}6H_2O$ (0.03 M) and VCl_3 (0.01 M) was added dropwise to10.0 mL of a $NaNO_3$ (0.01 M)

solution containing 23 vol % formamide. Simultaneously, a 0.75 M NaOH solution was likewise infused dropwise into maintaining the pH value of the reaction system at 10. After post-addition, the mixture was centrifuged, the precipitate was subjected to iterative deionized water washes until pH = 7 was achieved. The final solid product was collected and dried to obtain NiV-LDH.

To prepare the NiV-layered double oxide (NiV-LDO), a porcelain crucible loaded with 0.39 g of the as- synthesized NiV-LDH powder was inserted into a quartz tube reactor assembly. The system was purged with inert gas (e.g., N_2 or Ar) to remove residual air, and the protective gas flow rate was adjusted accordingly. The kiln temperature increased to 350 °C at a temperature ramp rate of 2 °C/min and lasted for 2 h. After cooling naturally to 25℃ in the same inert atmosphere, the calcined product was collected as NiV-LDO.

For the preparation of NiV-bimetallic phosphide (P-NiV), 2.64 g of NaH_2PO_2 was used as the phosphorus source and placed in a porcelain boat positioned at the upstream side of a tube furnace. Simultaneously, 0.39 g of NiV-LDH was placed in another porcelain boat located downstream. After properly sealing the furnace and purging with inert gas, the system was raised to 350 °C at a temperature ramp rate of 2 °C/min and lasted for 2 h to facilitate phosphating via vapor-phase transport. Upon chilling to room temperature under an inert atmosphere, the resulting black powder was collected as the final P-NiV catalyst.

2.4. Electrochemical measurements

The electrochemical testing was executed in a 1 M KOH aqueous electrolyte using a standard three-electrode quartz cell setup on an electrochemical workstation (CHI660, Chen Hua, Shanghai, China). The working electrodes were fabricated by drop-cast the synthesized NiV-LDH, NiV-LDO, or P-NiV onto a nickel foam (NF) substrate, respectively. The counter and reference electrodes consisted of a platinum mesh and an Ag/AgCl (saturated KCl) electrode, respectively. All recorded electrode potentials were referenced to the reversible hydrogen electrode (RHE) scale via the Nernst equation: $E_{RHE} = E_{Ag/AgCl} + 0.059pH + 0.197$. Linear sweep voltammetry (LSV) was conducted from 0 to 1 V vs. RHE at a scan rate of 5 mV s^{-1}. EIS measurements were performed at 0.5 V vs. RHE with a 10 mV AC amplitude, scanning frequencies from 100 kHz to 0.01 Hz. ECSA of the catalyst was determined from double-layer capacitance measurements in the non-Faradaic region (0.30–0.34 V vs. RHE). Cyclic voltammograms were recorded at scan rates of 2, 4, 6, 8, and 10 mV s^{-1}, with C_s extracted from the charging current–scan rate slope. ECSA was derived from the equation: $ECSA = C_{dl}/C_s$, where C_{dl} (double double-layer capacitance) is the slope of the CV curve and C_s is the specific capacitance of the sample.

2.5. Electrochemical measurements of phenol hydroxylation

The selective electrochemical hydroxylation of phenol to HQ was performed in an H-cell configuration divided by a Nafion-117 cation-exchange membrane. The anode consisted of the as-prepared catalyst coated on NF, while the cathode was a Pt mesh where hydrogen evolution occurred. Electrocatalytic phenol degradation was evaluated in 1 M KOH (50.0 mL) with 10 mM phenol under varied potentials (0.4–0.7 V vs. Ag/AgCl) and temperatures (25–50°C) for 9 h.

After the reaction, concentration profiles of phenol and its degradation products were monitored throughout electrochemical treatment by HPLC (Thermo Fisher U 3000) equipped with a C18(2) column and UV-Vis detector (λ=284 nm). The mobile phase was composed of a 1:1 (v/v) mixture of acetonitrile and deionized water., under isocratic conditions with 1 mL min^{-1} flow rate. Product identification was based on a comparison of retention times with standard reference compounds. The conversion of phenol (Xphenol) and the selectivity of its oxidation products (S) could be determined with the equations listed below:

$$X_{\text{phenol}} = \frac{\left(n^0_{phenol} - n^t_{phenol}\right)}{n^0_{phenol}} \times 100\%$$

$$S_{\text{Hydroquinone}} = \frac{n_{HQ}}{n_{HQ} + n_{CAT} + n_{BQ}} \times 100\%$$

where n^0_{phenol} is the initial phenol concentration, n^t_{phenol} denotes phenol concentration at given reaction times, and n_M represents the concentration of the oxidation products (M = hydroquinone (HQ), benzoquinone (BQ) and catechol (CAT)) at different stages of the reaction.

3. Results and discussion

The crystal structures of NiV-LDH, NiV-LDO, and P-NiV were determined by X-ray diffraction (XRD). Fig. 1a illustrates that the XRD pattern of NiV-LDH displayed characteristic Bragg reflections at 11.23°, 23.20°, 33.96°, and 60.12°, severally, matching the (003), (006), (009), and (110) crystal planes of typical LDHs, confirming the successful synthesis of NiV-LDH. According to the Bragg equation, the interlayer spacing of NiV-LDH is derived from calculations to about 0.788 nm, arising from the presence of interlayered CO_3^{2-} anions, as further supported by the Fourier-transform infrared (FTIR) spectroscopy. After calcination under an inert atmosphere, NiV-LDH was converted to NiV-LDO. The XRD pattern of NiV-LDO closely matches that of NiO (PDF#73-1523), although the characteristic peaks exhibit slight shifts. This deviation may be due to lattice distortion induced by the substitution of V ions into the NiO lattice. Upon phosphating, NiV-LDH was transformed into P-NiV. The diffraction pattern of P-NiV corresponds well with the standard pattern of Ni_2P (PDF#03-0953),[20] indicating that Ni_2P is the dominant phase. The substitution of some Ni atoms by V atoms is plausible, which may induce slight structural modifications within the Ni_2P lattice.

The FTIR spectra of NiV-LDH, NiV-LDO, and P-NiV are presented in Fig. 1b. For NiV-LDH, the broad absorption band at 3460 cm^{-1} is ascribed to the vibrational stretching of O-H bonds and interlayer water molecules. The 1640 cm^{-1} peak corresponds to water molecule bending vibrations, while the 1400 cm^{-1} band is assigned to asymmetric stretching vibrations of interlayer CO_3^{2-} ions. Additionally, the spectral feature below 1000 cm^{-1} originates from the metal oxygen (M-O) vibration. In comparison, absorption observed at 1640 cm^{-1} and 1400 cm^{-1} significantly diminish or disappear in NiV-LDO and P-NiV, indicating the effective removal of interlayer water, O-H groups, and carbonate species during calcination and phosphating processes.

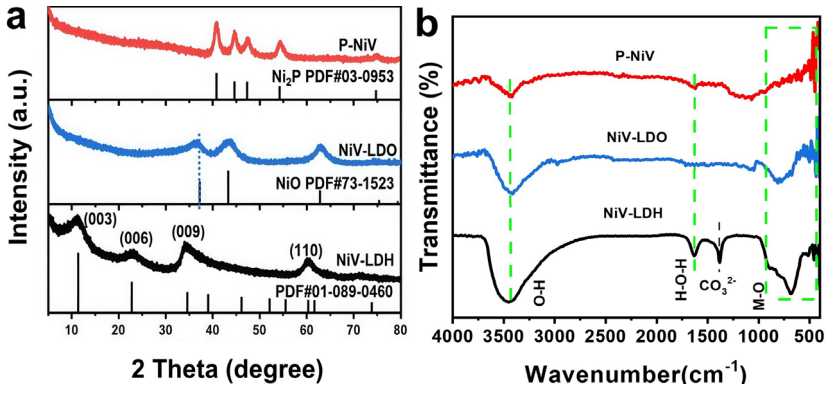

Fig. 1. (a) XRD patterns and (b) FT-IR spectra of NiV-LDH, NiV-LDO, and P-NiV.

Fig. 2 shows the scanning electron microscopy (SEM) and Energy-Dispersive X-ray spectroscopy (EDS) of the synthesized catalysts. As presented in Fig. 2a, NiV-LDH exhibits a well-defined two-dimensional layered structure, which is advantageous for facilitating high electrocatalytic performance. Fig. 2c and 2e reveal that both the thermally treated (NiV-LDO) and phosphate (P-NiV) samples retain the layered morphology of NiV-LDH, while exposing more active sites, thereby enhancing their electrocatalytic activity. Fig. 2b, 2d, and 2f indicate that the Ni/V atomic ratio of all catalysts are consistent with the theoretical feeding ratios, confirming the feasibility of the adopted synthetic methods. Notably, the proportion of phosphorus in P-NiV

increased significantly post-phosphating, with the metal-to-phosphorus ratio approaching 1:1, implying that electrical conductivity is not compromised.

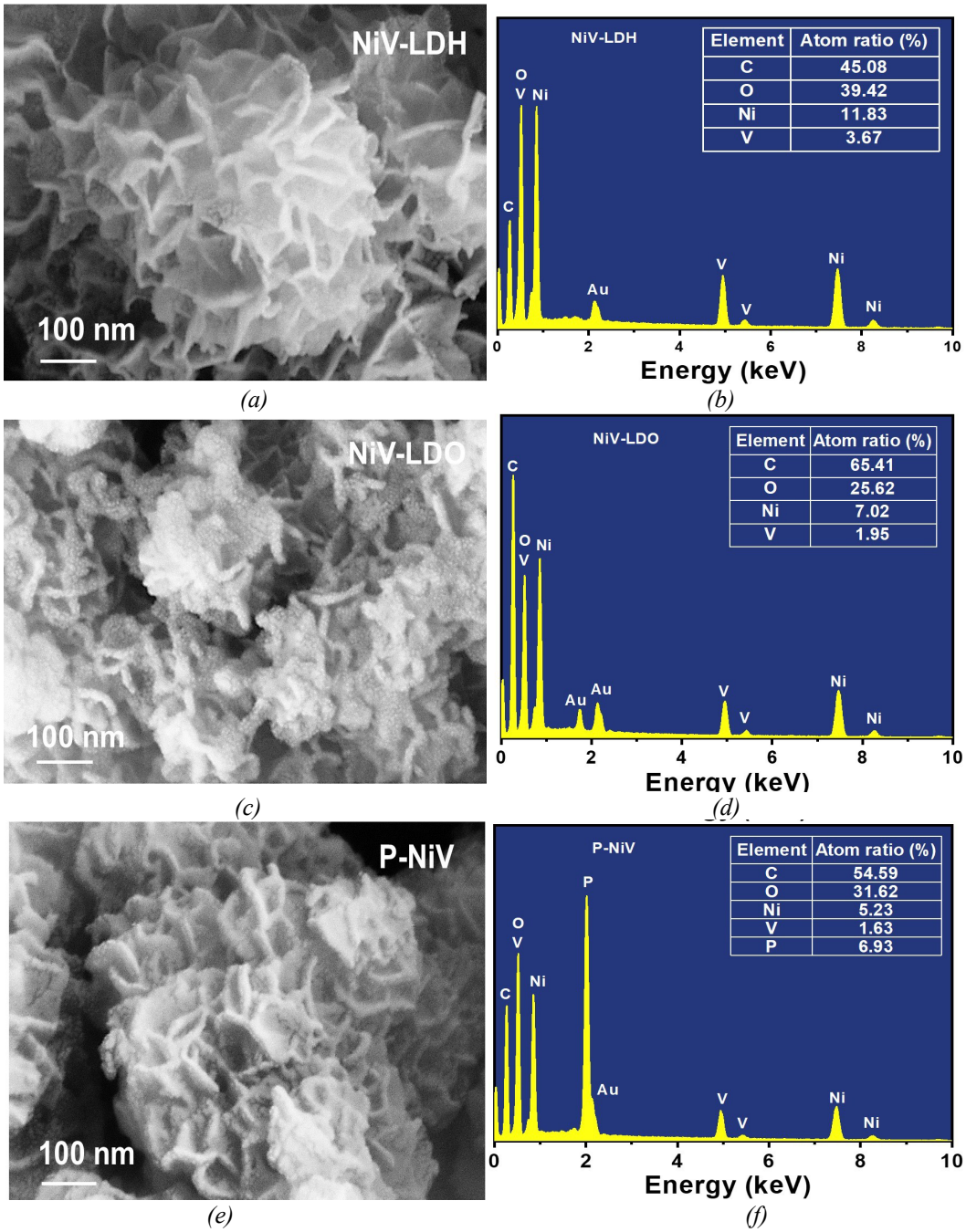

Fig. 2. SEM images of (a) NiV-LDH, (c) NiV-LDO, and (e) P-NiV; EDS spectra of (b) NiV-LDH, (d) NiV-LDO, and (f) P-NiV.

To investigate OER activity, electrocatalytic measurements were performed in 1 M KOH via a conventional three-electrode assembly at ambient temperature. As quantified by linear sweep voltammetry (LSV, Fig. 3a), the electrochemical behavior manifests P-NiV exhibits the lowest potential (1.46 V) at the same current density, highlighting its superior intrinsic activity. Electrochemical impedance spectroscopy (EIS, Fig. 3b) further confirms that P-NiV exhibits the smallest charge transfer resistance (R_{ct}), demonstrating faster reaction kinetics and enhanced charge

transport efficiency. Fig. 3c-3e displayed the CV curves at varying scan rates (2–10 mV·s^{-1} in 2 mV·s^{-1} increments). Double-layer capacitance (C_{dl}) values, quantified via linear fitting of current density differentials against scan rates, are presented in Fig. 3f. P-NiV exhibited the highest C_{dl} value (321 mF/cm^2), significantly surpassing that of NiV-LDH (164 mF/cm^2) and NiV-LDO (282 mF/cm^2). These results revealed that the P-NiV catalyst had a bigger electrochemically reactive interface and greater accessibility of catalytic centers.

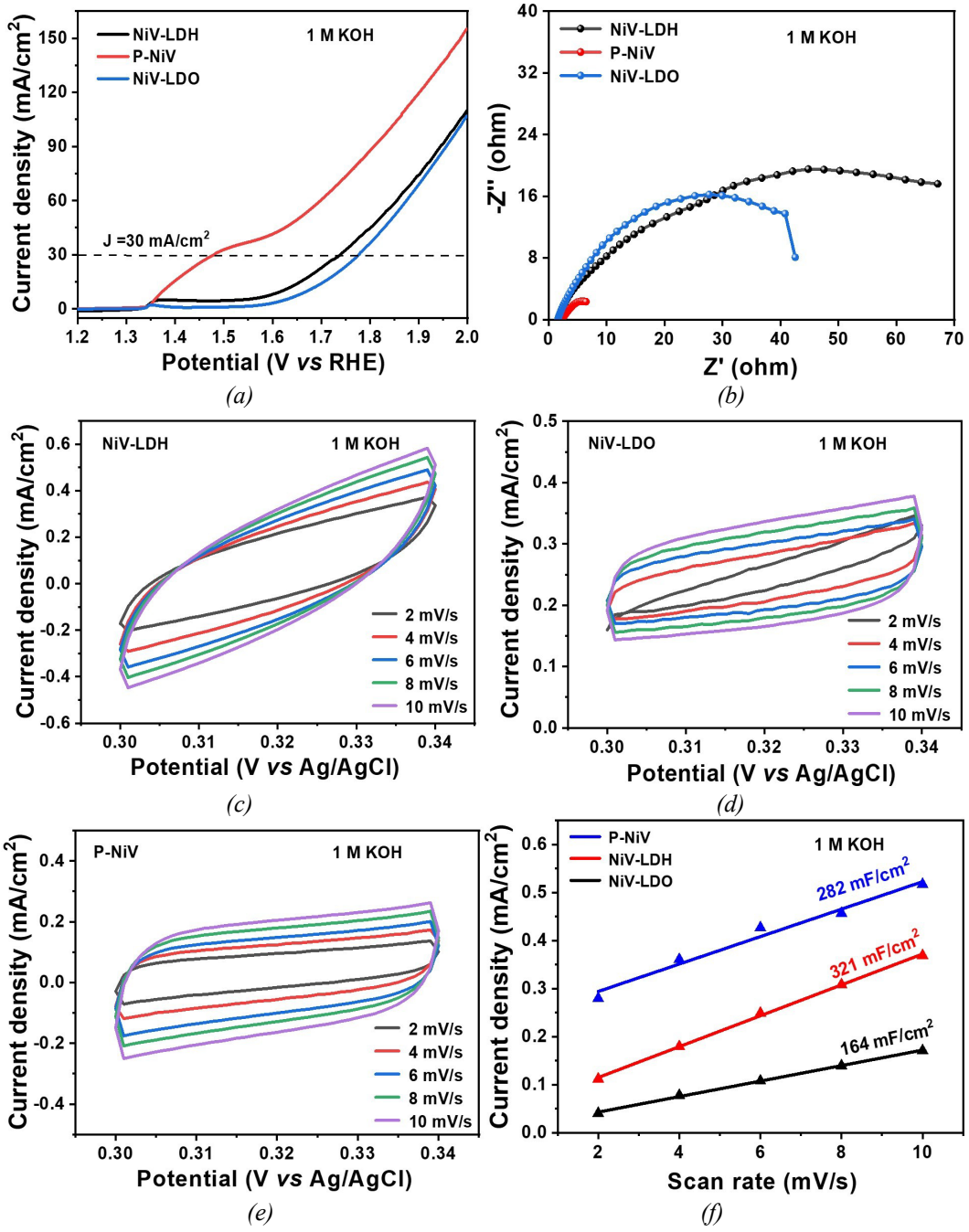

Fig. 3. (a) LSV curves, (b) EIS curves, and (f) C_{dl} values of NiV-LDH, NiV-LDO, and P-NiV; CV curves of (c) NiV-LDH, (d) NiV-LDO, and € P-NiV measured in 1 M KOH solution.

Given on the above findings, P-NiV was further investigated for electrocatalytic hydroxylation phenol in a solution of 1 M KOH containing 10 mM phenol.[21, 22] According to Fig. 4, P-NiV outperforms NiV-LDH and NiV-LDO, exhibiting the lowest onset potential, smallest R_{ct}, and highest C_{dl}, confirming its superior catalytic activity. The enhanced performance is likely due to improved specific conductance and increased availability of phenol- catalytic centers upon phosphating.

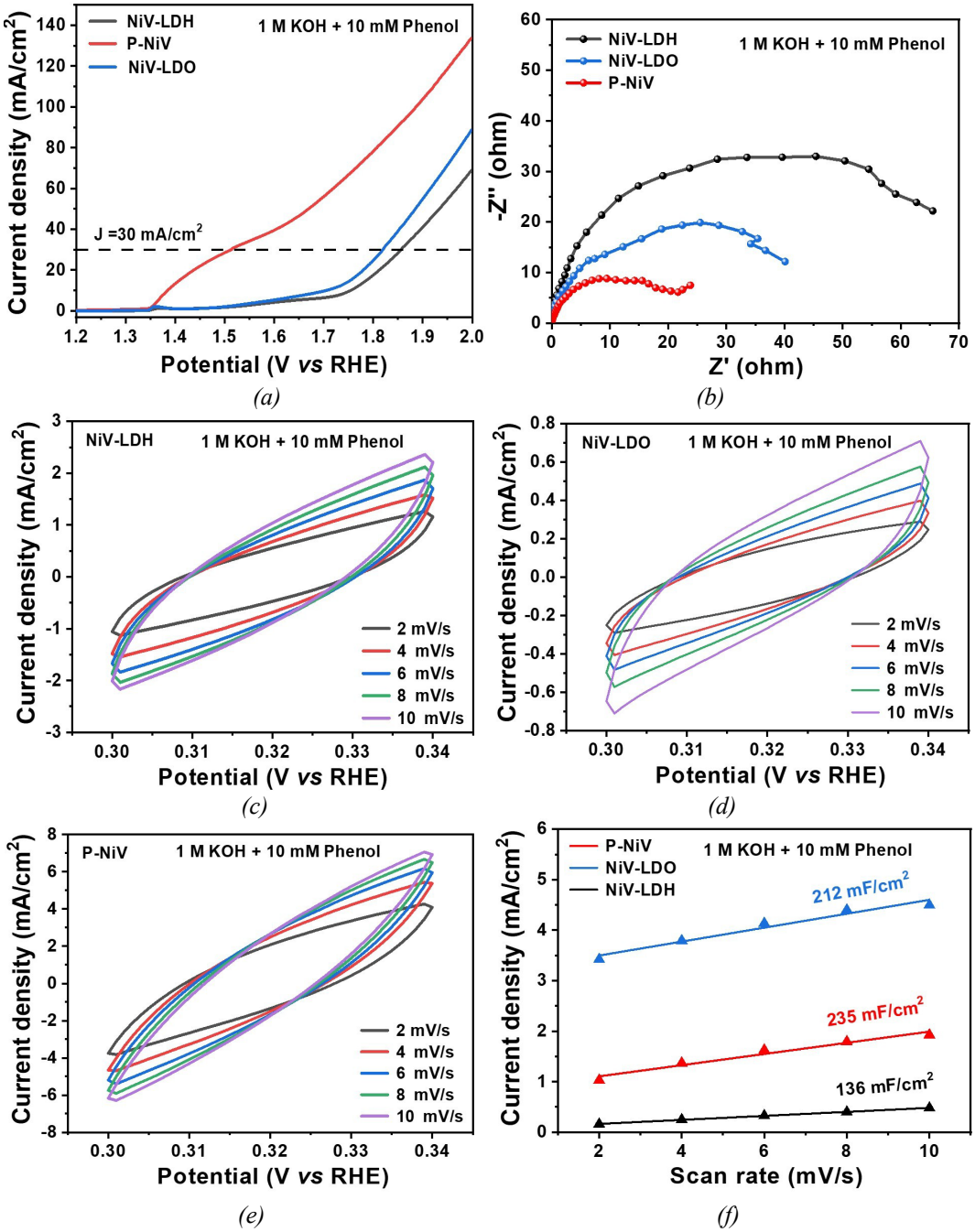

Fig. 4. (a) LSV curves, (b) EIS curves, and (f) C_{dl} values of NiV-LDH, NiV-LDO, and P-NiV; CV curves of (c) NiV-LDH, (d) NiV-LDO, and € P-NiV measured in 1 M KOH solution containing 10 mM phenol.

To optimize the reaction conditions, the effects of catalyst type, applied potentials, and reaction temperature on the electrocatalytic phenol hydroxylation were systematically studied, aiming to improve the phenol conversion and hydroquinone (HQ) selectivity. High performance liquid chromatography (HPLC) results (Fig. 5a) identified retention times of 2.56 min and 4.21 min for HQ and phenol, correspondingly. The phenol conversion and HQ selectivity were calculated based on concentration differences before and after electrolysis (Fig. 5b, 5c).

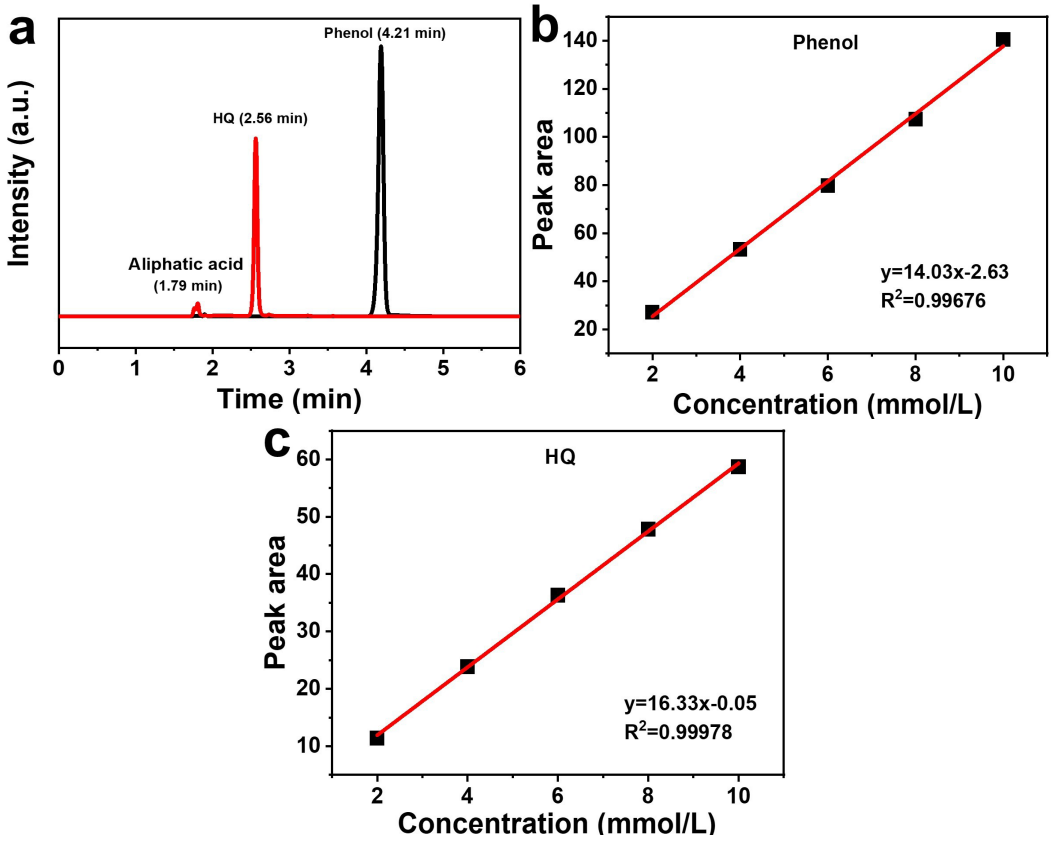

Fig. 5. (a) The HPLC spectra of phenol and its oxidative products; Standard curves of (b) phenol and (c) HQ.

By comparing the performance of NiV-LDH, NiV-LDO and P-NiV, P-NiV showed significant advantages. HPLC analysis in Fig. 6a showed that the phenol peak intensity significantly reduced, while that of HQ was considerably increased under P-NiV catalysis. Among the catalysts, P-NiV exhibited the highest phenol conversion (30.0 %) and HQ selectivity (70.0 %), outperforming NiV-LDH (16.5 %, 11.3 %) and NiV-LDO (16.8 %, 7.0 %) (Fig. 6b). The effect of applied potential (0.4-0.7 V) on phenol hydroxylation was further investigated (Fig. 6c and 6d). Although phenol conversion increased with potential and peaked at 0.7 V (38.0%), HQ selectivity decreased sharply to 32.4% due to competitive oxygen evolution. A balanced performance (conversion 30.0%, selectivity 70.0%) was achieved at 0.5 V, which was thus selected as the optimal potential. Furthermore, temperature studies revealed that phenol conversion increased from 30.0% at room temperature to 75.6% at 50 °C. However, HQ selectivity decreased to 56.1% due to overoxidation. At 40 °C, a suitable trade-off was reached with 57.7% conversion and 62.0% HQ selectivity (Fig. 6f). The presence of minor by-products was detected by stray peaks (3.1–3.3 min) in the HPLC spectra (Fig. 6e).

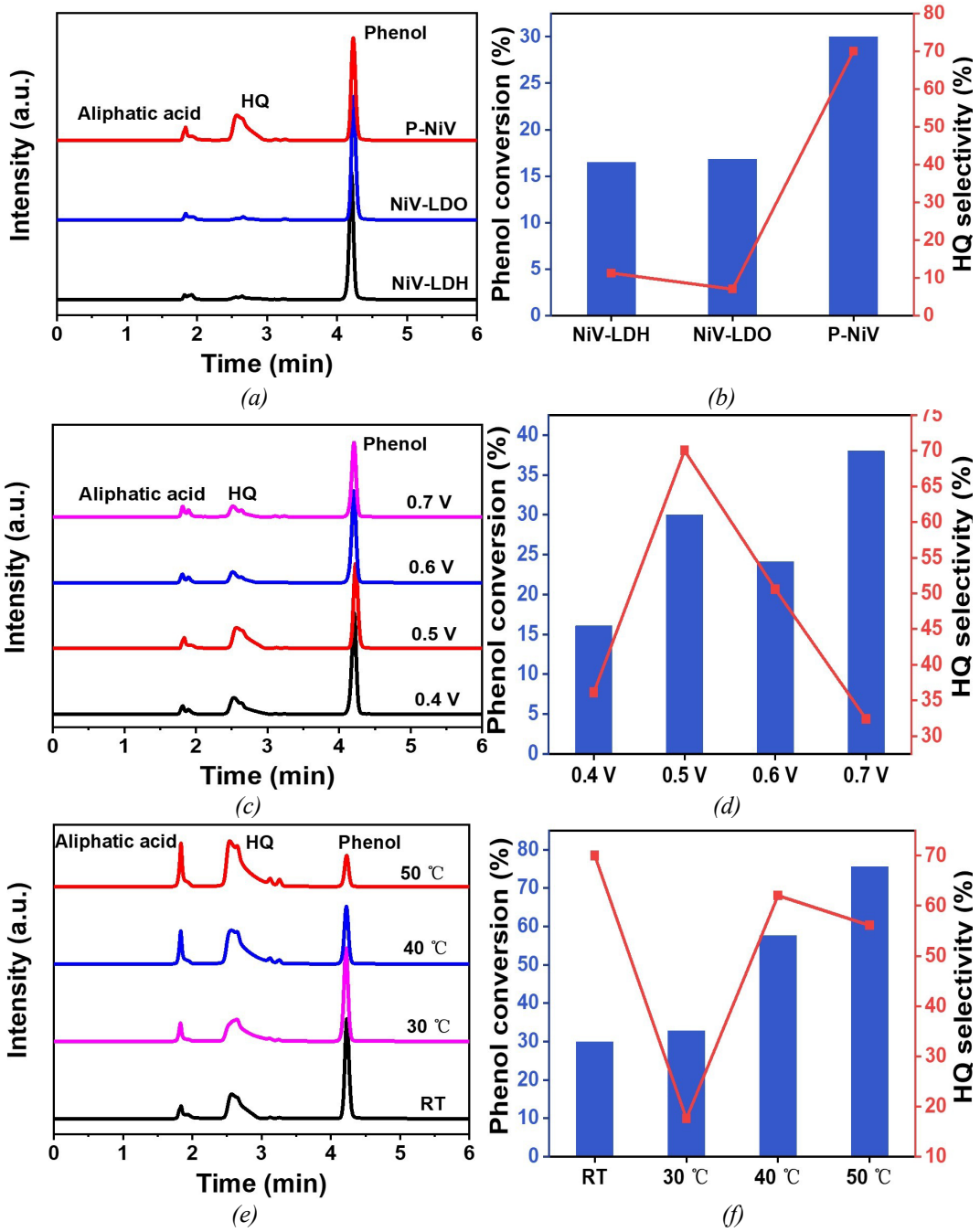

Fig. 6. HPLC spectra, phenol conversion and HQ selectivity: (a, b) RT, onset potential 0.5 V vs Ag/AgCl, reaction time 9 h, different catalysts; (c, d) P-NiV, RT, reaction time 9 h, different reaction initial potentials; (e, f) P-NiV, onset potential 0.5 V vs Ag/AgCl, reaction time 9 h, different reaction temperatures.

4. Conclusion

In summary, a novel nickel–vanadium bimetallic phosphide (P-NiV) electrocatalyst was successfully synthesized via phosphating of NiV-layered double hydroxide (NiV-LDH), following a topological transformation process. Structural characterizations confirmed that P-NiV retained the two-dimensional layered morphology of the LDH precursor while exhibiting enhanced electronic conductivity and stability. These improvements are attributed to the phosphating-induced modulation of surface-active sites and enhanced electron transport properties. Electrochemical evaluations using a three-electrode system demonstrated that, among the three catalysts tested (NiV-

LDH, NiV-LDO, and P-NiV), the P-NiV catalyst exhibited superior activity for phenol hydroxylation. Under optimized conditions (applied potential of 0.5 V and temperature of 40 °C), P-NiV achieved a phenol conversion of 57.7% and hydroquinone (HQ) selectivity of 62%. Compared with conventional thermal methods, this electrocatalytic approach offers a green, energy-efficient, and selective strategy for phenol hydroxylation. The findings provide a theoretical and practical foundation for the development of sustainable catalytic systems for fine chemical synthesis.

Acknowledgements

This research was supported by funding of the Guangxi Natural Science Foundation (No. 2023GXNSFBA026183, No. 2025GXNSFAA069404), the Open Project of Guangxi Key Laboratory of Nuclear Physics and Nuclear Technology (No. NLK2022-08), and the National Innovation and Entrepreneurship Training Program for college students (No. 202510596029).

References

[1] R. Molinari, P. Argurio, T. Poerio, Applied Catalysis A, General **437**, 131 (2012); https://doi.org/10.1016/j.apcata.2012.06.027

[2] G. Vega, A. Quintanilla, M. Belmonte, J. Casas, Chemical Engineering Journal **428**, 131128 (2022); https://doi.org/10.1016/j.cej.2021.131128

[3] S. Yusuf, A. Moheb, M. Dinari, Research on Chemical Intermediates **47**, 1297 (2021); https://doi.org/10.1007/s11164-021-04402-0

[4] Y. Jiang, W.-L. Xu, J.-C. Liang, J.-C. Shen, X.-M. Fu, H.-M. He, S.-C. Yan, X.-Q. Ren, New Journal of Chemistry **45**(1), 179 (2020); https://doi.org/10.1039/D0NJ03905E

[5] G. S. Buzzo, A.C.B. Rodrigues, R.F.B. De Souza, J.C.M. Silva, E.L. Bastos, A.O. Neto, Catalysis Communications **59**, 113 (2014); https://doi.org/10.1016/j.catcom.2014.09.048

[6] C. Li, Y. Nakagawa, M. Tamura, A. Nakayama, K. Tomishige, ACS Catalysis **10**(24), 14624 (2020); https://doi.org/10.1021/acscatal.0c04336

[7] L. Zhang, Y. Fang, Z. Du, D.-D. Bi, Z.-L. Guo, Z.-Y. Liu, Y. Huang, J.Lin, C.-C. Tang, ChemistrySelect **6**(24), 5975 (2021); https://doi.org/10.1002/slct.202101314

[8] B. Lee, H. Naito, T. Hibino, Angewandte Chemie International Edition **51**(2), 440 (2011); https://doi.org/10.1002/anie.201105229

[9] G. Luo, X.-C. Lv, X.-W. Wang, S. Yan, X.-H. Gao, J. Xu, H. Ma, Y.-J. Jiao, F.-Y. Li, J.-Z. Chen, RSC Advances **5**(114), 94164 (2015); https://doi.org/10.1039/C5RA17287J

[10] S. Farahmand, M. Ghiaci, S. Asghari, Chemical Engineering Science **232**, 116331 (2021); https://doi.org/10.1016/j.ces.2020.116331

[11] M. R. Maurya, N. Jangra, F. Avecilla, N. Ribeiro, I. Correia, ChemistrySelect **4**(43), 12743 (2019); https://doi.org/10.1002/slct.201903678

[12] T. Li, J.-Y. Mo, D. M. Weekes, K. E. Dettelbach, R. P. Jansonius, G. N. Sammis, C. P. Berlinguette, ChemSusChem **13**(14), 3622 (2020); https://doi.org/10.1002/cssc.202001134

[13] W.-Z. Huang, C.-X. Chen, Z.-H. Ling, J.-T. Li, L.-B. Qu, J.-X. Zhu, W. Yang, M.-M. Wang, K. A. Owusu, L. Qin L. Zhou, L.-Q. Mai, Chemical Engineering Journal **405**, 126959 (2020); https://doi.org/10.1016/j.cej.2020.126959

[14] Y.-J. Qi, Y.-H. Wang, H.-M. Li, M.-H. Cao, C.-W. Hu, E.-B. Wang, N.-H. Hu, H.-Q. Jia, Journal of Molecular Structure **650**(1-3), 123 (2003).

[15] J.-J. Lv, P.-P. Liu, F. Yang L.-W. Xing, D.-N. Wang, X.Chen, H.-Y. Gao, X.-B. Huang, Y.-F. Lu, G. Wang, ACS Applied Materials & Interfaces **12**(43), 48495 (2020); https://doi.org/10.1021/acsami.0c11722
[16] Y.-Z. Li, B. Wei, M.-H. Zhu, J.-C. Chen, Q.-K. Jiang, B.Yang, Y. Hou, L.-C. Lei, Z.-J. Li, R.-F. Zhang, Y.-Y. Lu, Advanced Materials **33**(41), 2102212 (2021); https://doi.org/10.1002/adma.202102212
[17] T. Mudrinić, Z. Mojović, A. Milutinović-Nikolić, P.Banković, B. Dojcinović, N. Vukelić, D. Jovanović, Electrochimica Acta **144**, 92 (2014); https://doi.org/10.1016/j.electacta.2014.07.115
[18] G. E. Ayom, M. D. Khan, S. C. Masikane, F. M. de Souza, W. Lin, R. K. Gupta, N. Revaprasadu, Sustainable Energy & Fuels **6**(5), 1319 (2022); https://doi.org/10.1039/D1SE01866C
[19] Y.-Q. Xu, H.-J. Liu, Y.-X. Wu, Q. Wu, C.-J. Li, X.-Y. Wang, H.-Q. Qin, A.-M. Qin, L.-J. Wang, ChemNanoMat **9**(12), e202300414 (2023); https://doi.org/10.1002/cnma.202300414
[20] J.-S. Yan, H.-B. Liu, Y. S. E., F.-W. He, IOP Conference Series Materials Science and Engineering **292**, 012119 (2018); https://doi.org/10.1088/1757-899X/292/1/012119
[21] J.-W. Nai, X.-Z. Xu, Q.-F. Xie, G.-X. Lu, Y. Wang, D.-Y. Luan, X.-Y. Tao, Advanced Materials **34**(4), 2104405 (2021); https://doi.org/10.1002/adma.202104405
[22] W.-R. Cheng, H.-B. Zhang, D.-Y Luan, X.-W. Lou, Science Advances **7**(18), eabg2580 (2021); https://doi.org/10.1126/sciadv.abg2580